Applied Energy 190 (2017) 540–552

Contents lists available at ScienceDirect

Applied Energy

journal homepage: www.elsevier.com/locate/apenergy

Geometry optimization of two-stage thermoelectric generators using simplified conjugate-gradient method

Zhichun Liu [a,*], Shiping Zhu [a], Ya Ge [a], Feng Shan [a], Lingping Zeng [b], Wei Liu [a,*]

[a] School of Energy and Power Engineering, Huazhong University of Science and Technology, Wuhan 430074, China
[b] Department of Mechanical Engineering, Massachusetts Institute of Technology, Cambridge, MA 02139-4307, United States

HIGHLIGHTS

- Integrating computer-aided analysis with an optimization method to design and optimize TEGs.
- Obtaining multi-objective and multi-parameter optimization of structure for a two-stage TEG module.
- Properly balancing the power output and conversion efficiency to improve them simultaneously.

ARTICLE INFO

Article history:
Received 23 September 2016
Received in revised form 2 January 2017
Accepted 3 January 2017
Available online 9 January 2017

Keywords:
Thermoelectric generator
Power output
Conversion efficiency
Multi-objective
Multi-parameter
Optimization

ABSTRACT

Thermoelectric devices can convert thermal energy directly into electrical energy. The aim of this study was to develop an approach for integrating computer-aided analysis with an optimization method that could be applied to the design and optimization of thermoelectric generators. The optimization framework consisted of a model generator, a direct solver, and a numerical optimizer. The simplified conjugate-gradient method (SCGM) was used to build the optimizer, and the general-purpose finite-element code was used for the direct solver and model generator. This approach was applied to the multi-objective and multi-parameter optimization of geometric thermoelectric generators to design an optimal structure for both a two-stage bismuth-telluride (BiTe)-based and skutterudite-based thermoelectric generator (TEG) module. The leg length and the ratio between the cross-sectional areas (i.e., footprint) of the semiconductor columns and the TEG module were found to significantly affect the TEG performance; hence, all were incorporated into the present optimization study. Multi-objective optimization was used to realize a design that properly balanced the power output and conversion efficiency so that both improved simultaneously.

1. Introduction

Thermoelectric generator (TEG) operation is based on the Seebeck effect, which allows semiconductors to directly convert thermal energy to electricity [1,2]. Because thermoelectric energy conversion is based completely on solid-state technology and has no moving parts or environmentally harmful fluids, it has the unique advantages of high reliability and quiet, environmentally friendly operation [3]. Research and development for TEG systems has mostly been disconnected to the parametric optimization of the module components, and most related studies have involved engineering parametric analysis [4–7]. Previous performance studies have shown that the TEG power output and conversion efficiency are strongly dependent on their semiconductor material properties [8–13]. In general, the dimensionless figure of merit (ZT) represents the thermoelectric performance of the device, which is defined as $ZT = \alpha^2\sigma T/\lambda$, where α is the Seebeck coefficient, σ is the electrical conductivity, λ is the thermal conductivity, and T is the absolute temperature at which the properties are measured [14]. A larger ZT represents a better thermoelectric device performance. Therefore, the majority of thermoelectric research has focused on improving the ZT of the material without considering other factors such as interfacial bonding materials, weight, cost-effectiveness, and environmental damage. The performance of thermoelectric modules has been modeled for various applications such as automotive [15,16], internal combustion engines [17], and space travel [18].

Some studies have found that the geometric structure of a thermoelectric device has a remarkable effect on TEG performance [19–24]. Chen et al. [20] proposed a new cycle model that consisted of a multi-couple thermoelectric device and involved several

* Corresponding authors.
E-mail addresses: zcliu@hust.edu.cn (Z. Liu), w_liu@hust.edu.cn (W. Liu).

http://dx.doi.org/10.1016/j.apenergy.2017.01.002
0306-2619/

Nomenclature

P	power output (W)
η	conversion efficiency
COP	coefficient of performance
ZT	figure of merit
T	temperature (K)
T_h	hot-side temperature
T_c	cold-side temperature
f	weight factor
C	search variable
A_{total}	area of TEG module base
J	objective function
A_{pn}	cross-sectional area of p- or n-type semiconductor
H	height (mm)
H_{pn}	height of element (leg length), equal to HpnL as the search variable
H_{pnL}	height of lower stage element (leg length)
H_{pnU}	height of upper stage element (leg length)
W	width (mm)

Abbreviation

TEG	thermoelectric generator
TEC	thermoelectric cooler

Greek letters

α	seebeck coefficient ($V K^{-1}$)
σ	electrical conductivity ($S m^{-1}$)
λ	thermal conductivity ($W m^{-1} K^{-1}$)
ρ	electric resistivity (Ωm^{-1})
Δ	difference
B	search step size
π	search direction
γ	area ratio of An/Ap

Subscripts

opt	optimal
p, n	p- or n-type semiconductor
Cu	copper
k	number of variables
L	lower stage
U	upper stage

Superscript

n	number of iterations

key irreversibilities of real TEGs. They used the model to optimize the performance of a multi-couple TEG and discussed the optimal structure for a TEG. Chen [19] investigated the theoretical maximum efficiency of a solar TEG by using the Lagrangian multiplier method. For a single TEG module with a fixed base area, the geometric parameters include the leg length and the footprint area. All parameters have a coupled effect on TEG performance. Jang et al. [25] adopted a single-parameter method to study how the foot length and cross-sectional area of the p- or n-type semiconductor affected the performance of a micro-TEG uni-couple. They found that, for each of the three geometrical parameters, there was always a specific parameter corresponding to the optimal power output or conversion efficiency; however, the optimal power output and conversion efficiency values could not be reached simultaneously. An individual parameter study is useful but cannot obtain the optimal TEG structure. The optimal value for a specific parameter is obtained by varying the parameter to reach the optimal thermoelectric performance while keeping the other parameters fixed; however, because all the parameters have coupled effects on thermoelectric performance, the optimal thermoelectric performance cannot be reached by varying a single specific parameter. Several studies have tried to develop a multi-objective optimization method by combining an optimization algorithm with a TEG/TEC numerical model [22,23,26,27]. Meng et al. combined a TEG model and a simplified conjugate-gradient (SCG) to optimize the leg length, base area ratio, and number of legs simultaneously [27]. Huang et al. [26] combined a multi-physics thermoelectric cooler (TEC) model and an SCG algorithm to optimize the cooling capacity of a TEC module. The semiconductor pair number, leg length, and base area ratio of the semiconductor elements were chosen as search variables. The optimal geometry under the maximum cooling capacity was obtained; however, the coefficient of performance (COP) of the optimal geometry was reduced compared with that of the initial geometry.

Apart from the module geometric design, the co-design of the thermoelectric module in conjunction with the thermal boundary conditions also plays an important role in improving system performance. Few works have considered the effect of heat dissipation on the cold side. Some studies [28,29] developed parametric analysis methods for exothermic systems that used an optimal design model. These studies focused on heat dissipation but used identical material properties; however, n- and p-type thermoelectric materials are not naturally identical. Most theoretical studies were limited to one-dimensional models [30], or their thermoelectric elements were considered to be identical materials, so the differences between the thermal and electrical resistances of the thermoelectric elements were not accurately evaluated [31]. Moreover, the power factors of the n- and p-type elements differ because the Seebeck coefficient and electrical resistance of the materials depend on temperature [32]. In an earlier study, Row and Min [33] studied the effect of the thermoelectric uni-couple area on power generation by using several commercially available modules with equal footprints; the footprint is another important factor for power generation. However, they used a constant temperature as a boundary condition on the cold side of the modules, which does not reflect reality.

To improve the volumetric power generation of a TEG, this study presents an approach to find the optimal TEG geometry that integrates a multi-physics TEG model and an SCG method. The approach was used to optimize a TEG module. The weighted average of P and η was taken as the multi-objective function to optimize two search variables (i.e., two-stage leg length and footprint of n- and p-type elements) simultaneously to determine the optimal TEG performance. Parametric optimization was performed on a TEG uni-couple that considered the temperature-dependent properties of the thermoelectric materials. The maximum power generation and optimal efficiency of the two-stage uni-couples were evaluated under a matched-load condition and over a wide range of n/p footprint ratios and leg lengths, while the total footprint and leg length of the two-stage elements were kept constant.

2. Optimization approach

2.1. Schematic of TEG

Fig. 1 shows the schematic of a TEG with a base area of $A_{base} = 5 \times 6\ mm^2$. The two-stage uni-couple includes a p-type semiconductor column and an n-type semiconductor column on each stage, six metallic interconnectors, and three electrical insulation ceramic plates. The p- and n-type semiconductors of each stage have the same height and footprint: $H_{nL} = H_{pL} = H_{pnL}$, $H_{nU} = H_{pU} = H_{pnU}$, $H_{pnL} + H_{pnU} = 4$ mm, $A_{nL} = W_{nL} \times W_{nL}$, $A_{pL} = W_{pL} \times W_{pL}$, $A_{nL} + A_{pL} = 8\ mm^2$, $A_{nU} = W_{nU} \times W_{nU}$, $A_{pU} = W_{pU} \times W_{pU}$, and $A_{nU} + A_{pU} = 8\ mm^2$. The Seebeck coefficients, electrical conductivities, and thermal conductivities of the p- and n-type materials in a TEG are different. Thus, an optimized TEG design should have different cross-sectional areas for the p- and n-type semiconductor columns. Once the footprint and leg length H_{pn} are given, the unit of the TEG geometric structure is determined. Thus, these two parameters were chosen as search variables and were optimized simultaneously to reach the maximum power generation and maximum efficiency. The application ranges for the n-Sku, p-Sku, n-BiTe, and p-BiTe were approximately 300–850 °C, 300–800 °C, 300–500 °C, and 300–550 °C, respectively [34,35]. All material properties, including thermal conductivity, electrical conductivity, Seebeck coefficient, and ZT value were selected based on those given in [34,35]. For convenience of calculation, the properties were fitted into polynomials with temperature.

2.2. Optimization approach

The 3D TEG model was adopted as a direct problem model. The model assumed the following: the TEG operates at a steady state, the TEG uni-couple is connected electrically in series and thermally in parallel, electrical insulation ceramics (top, middle, and bottom) have excellent thermal conductivity, the material properties of the TEG are temperature-dependent, the thermal and electrical contact resistances between the semiconductor columns and metallic interconnectors can be neglected, and the heat losses by radiative and convective heat transfer to the ambient can be neglected. The heat conduction and electric potential equations of the model are described briefly below. More details are given in [27].

The power of a TEG uni-couple was used as the objective function. The maximum power output can be reached by determining the optimal parameter combination of H_{pn}, and A_n/A_p, but this may reduce the conversion efficiency. Similarly, the maximum conversion efficiency is reached when the power output is not at its maximum. Therefore, the power output and conversion efficiency of the TEG module were considered simultaneously for multi-objective optimization. In this study, the multi-objective function is defined as follows [36]:

$$J = 1 \Big/ \left(f\frac{P}{P_{opt}} + \left(1 - f\frac{\eta}{\eta_{opt}}\right)\right)_0 \tag{1}$$

where f is a weight factor for the first objective function P, and P_{opt} and η_{opt} are the maximum values of the objective functions P and η, respectively, when these objectives are maximized independently.

2.3. Governing equations

2.3.1. Heat-conduction equations

$$\nabla \cdot (\lambda_i \nabla T) + \frac{j^2}{\sigma_i} - \beta_i \vec{j} \cdot \nabla T = 0 \tag{2}$$

$$\nabla \cdot (\lambda_p \nabla T) + \frac{j^2}{\sigma_p} - \beta_p \vec{j} \cdot \nabla T = 0 \tag{3}$$

$$\nabla \cdot (\lambda_n \nabla T) + \frac{j^2}{\sigma_n} - \beta_n \vec{j} \cdot \nabla T = 0 \tag{4}$$

2.3.2. Electric-potential equation

$$\nabla \cdot (\sigma(\nabla \varphi - \alpha \nabla T)) = 0 \tag{5}$$

In the above equations, λ is the thermal conductivity, σ is the electrical conductivity, β is the Thomson coefficient, $\vec{j}$ is the current density vector, α is the Seebeck coefficient, and φ is the electric potential. The subscripts i, p, and n denote the interconnector, p-type semiconductor, and n-type semiconductor, respectively. The Thomson coefficient is related to the Seebeck coefficient as follows:

$$\beta = T\frac{d\alpha}{dT} \tag{6}$$

Once the electric potential is obtained, the current density vector can be calculated by the following equation:

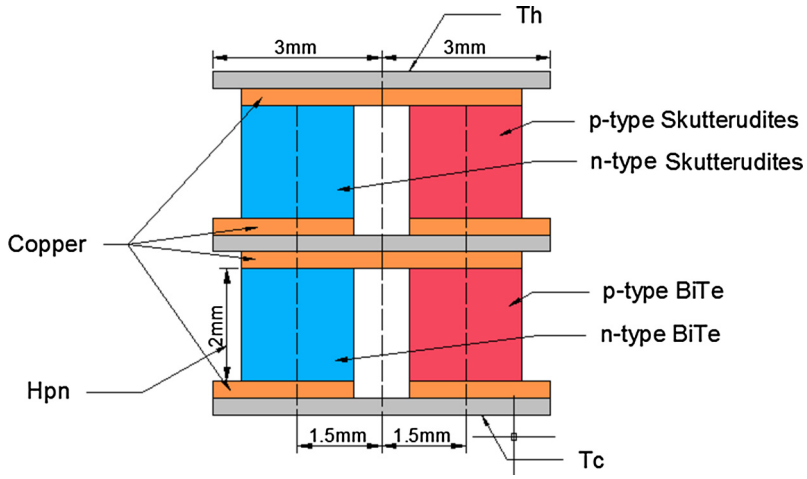

Fig. 1. Schematic of TEG uni-couple.

$$\vec{j} = \sigma \vec{E} = \sigma(-\nabla\varphi + \alpha\nabla T) \tag{7}$$

The open-circuit voltage and short-circuit current in a TEG uni-couple are as follows:

$$V_{oc} = \overline{\alpha}\Delta T \tag{8}$$

$$I_{sc} = \frac{\overline{\alpha}\Delta T}{R} \tag{9}$$

The average Seebeck coefficient of the uni-couple is as follows [37]:

$$\overline{\alpha} = \frac{1}{T_h - T_c}\int_{T_c}^{T_h}(\alpha_p - \alpha_n)dT \tag{10}$$

The internal resistance of the uni-couple in Eq. (9) is as follows [38]:

$$R = R_n + R_p = \left[\left(\sigma_n \frac{A_n}{H_n}\right)^{-1} + \left(\sigma_p \frac{A_p}{H_p}\right)^{-1}\right] \tag{11}$$

The maximum power generated by the uni-couple can be calculated from the optimal current and electric voltage generated in the uni-couple that occurs at half of the short-circuit current and half of the open-circuit voltage. This is the matched-load condition, where the internal electrical resistance of the uni-couple is equal to the imposed electrical load resistance [39,40].

$$P_{\max} = v_{opt} \times I_{opt} = \frac{(\Delta T\overline{\alpha})^2}{4R}\left(\sigma_n \frac{A_n}{H_n}\right)^{-1} \tag{12}$$

The efficiency of the uni-couple is the ratio of the power provided to the load and the heat absorbed at the hot junction:

$$\eta = \frac{P}{Q} = \frac{T_h - T_c}{T_h}\cdot\frac{\sqrt{1+ZT_m}-1}{\sqrt{1+ZT_m}+T_c/T_h} \tag{13}$$

2.4. Constraint and boundary conditions

The thermoelectric elements of each stage were 2 mm long, while the footprint ratios and length of the squared n/p elements of each stage were initially considered equal: $H_{pL} = H_{nL} = 2$ mm, $H_{pU} = H_{nU} = 2$ mm, and $H_{pL} + H_{pU} = 4$ mm. The element length on each stage was always the same. The total area of the n/p footprints ($A_n + A_p$) was fixed at 8 mm^2 for all designed uni-couples. The area of the identified ceramic substrate of each thermoelectric element was 3×3 mm^2. Thus, the distance between the center points of the thermoelectric elements was 3 mm as shown in Fig. 1. The thickness of the ceramic substrate and copper interconnectors was 0.3 mm.

To realize a practical approach, the search variables should be considered over a reasonable range. Because of the limitations of actual processing, H_p and H_n cannot be arbitrarily small, nor can the cross-sectional area A also be too small. To minimize processing difficulties, the constraint conditions for the optimization were chosen to be $H_{pn} > 0.3$ mm and A_n or $A_p > 0.5$ mm^2.

Constant temperatures T_h and T_c were applied to the hot and cold sides, respectively, of the TEG. The temperature and heat flux were assumed to be continuous on the interface between the interconnector and semiconductor and the electrical insulation ceramic plates. The adiabatic boundary condition was assumed for the side surfaces of the TEG.

In single-parameter analysis, only one parameter of interest changes while the other two parameters keep the values of the initial geometry. For a TEG module with a fixed substrate, once the semiconductor leg length (H_{pn}) and the cross-sectional area ratio of the semiconductor columns on each stage are specified, the two-stage TEG module geometry is uniquely determined. Fig. 2 shows the effect of a single parameter H_{pn}, $\gamma_L = A_{nL}/A_{pL}$, or $\gamma_U = A_{nU}/A_{pU}$ on the TEG module performance at different temperatures. *L* represents the lower stage, and *U* represents the upper stage.

The cold-side temperature was assumed to be 293 K, and the hot-side temperature was varied from 493 to 973 K. The baseline geometry was defined as $H_{pn} = 2$ mm, $\gamma_L = A_{nL}/A_{pL} = 1$, and $\gamma_U = A_{nU}/A_{pU} = 1$. In single-parameter analysis, only one parameter changes while the other two parameters do not change. We found that H_{pn}, $\gamma_L = A_{nL}/A_{pL}$, and $\gamma_U = A_{nU}/A_{pU}$ significantly affected the TEG module power output and efficiency. Consequently, these three parameters were chosen as the search variables.

2.5. Optimization procedure

The optimization procedure steps for applying the SCG algorithm are described briefly below. For convenience, search variables C_1, C_2, and C_3 were used to denote the semiconductor leg length H_{pn} (as shown in Fig. 1), lower stage footprint ratio γ_L, and upper stage footprint ratio γ_U, respectively.

(1) Estimate initial values for the search variables C_1, C_2, and C_3 and the values of the search step sizes β_1, β_2, and β_3.
(2) Create the geometry and grids of the TEG using the specified search variables C_1, C_2, and C_3. Set up all boundary conditions and then numerically solve Eqs. (1)–(13).
(3) Evaluate the objective function *J*. When the convergence criterion is satisfied, the objective function reaches the minimum. At this point, terminate iteration; otherwise, proceed to step (4).
(4) Determine the gradient functions $(\partial J/\partial C)^n$ of the objective function for each search variable based on the following equation:

$$\frac{\partial J}{\partial C} = \frac{\Delta J}{\Delta C} \tag{14}$$

(5) Calculate the conjugate-gradient coefficients γ and search directions π for each search variable.

$$\gamma^{(n)} = \left[\frac{(\partial J/\partial C)^{(n)}}{(\partial J/\partial C)^{(n-1)}}\right]^2 \tag{15}$$

$$\pi^{(n+1)} = \left(\frac{\partial J}{\partial C}\right)^{(n)} + \gamma^{(n)}\pi^{(n-1)} \tag{16}$$

where the superscripts n and $n-1$ denote the number of search steps. For $n = 1$, $\gamma = 0$.

(6) Update the new search variables:

$$C^{(n+1)} = C^{(n)} - \beta\pi^{(n)} \tag{17}$$

and then return to step (2).

Typical values for ΔH and ΔA were 0.01 mm and 0.0001 mm^2, respectively. β varied from 0.001 to 0.06 depending on the convergence situation during the optimization. Fig. 3 shows a flowchart of the optimization. The TEG model was solved with COMSOL, and the SCG model was solved by a live-link with MATLAB.

Like other gradient algorithms, the SCGM may not find the global minimum of the objective function because it may be trapped in local minima. The results of the SCGM depend on the set of initial parameters. Thus, several trials may be required to find the global minimum solution. For this reason, three different sets of initial search variable values were used to validate the optimization in this study.

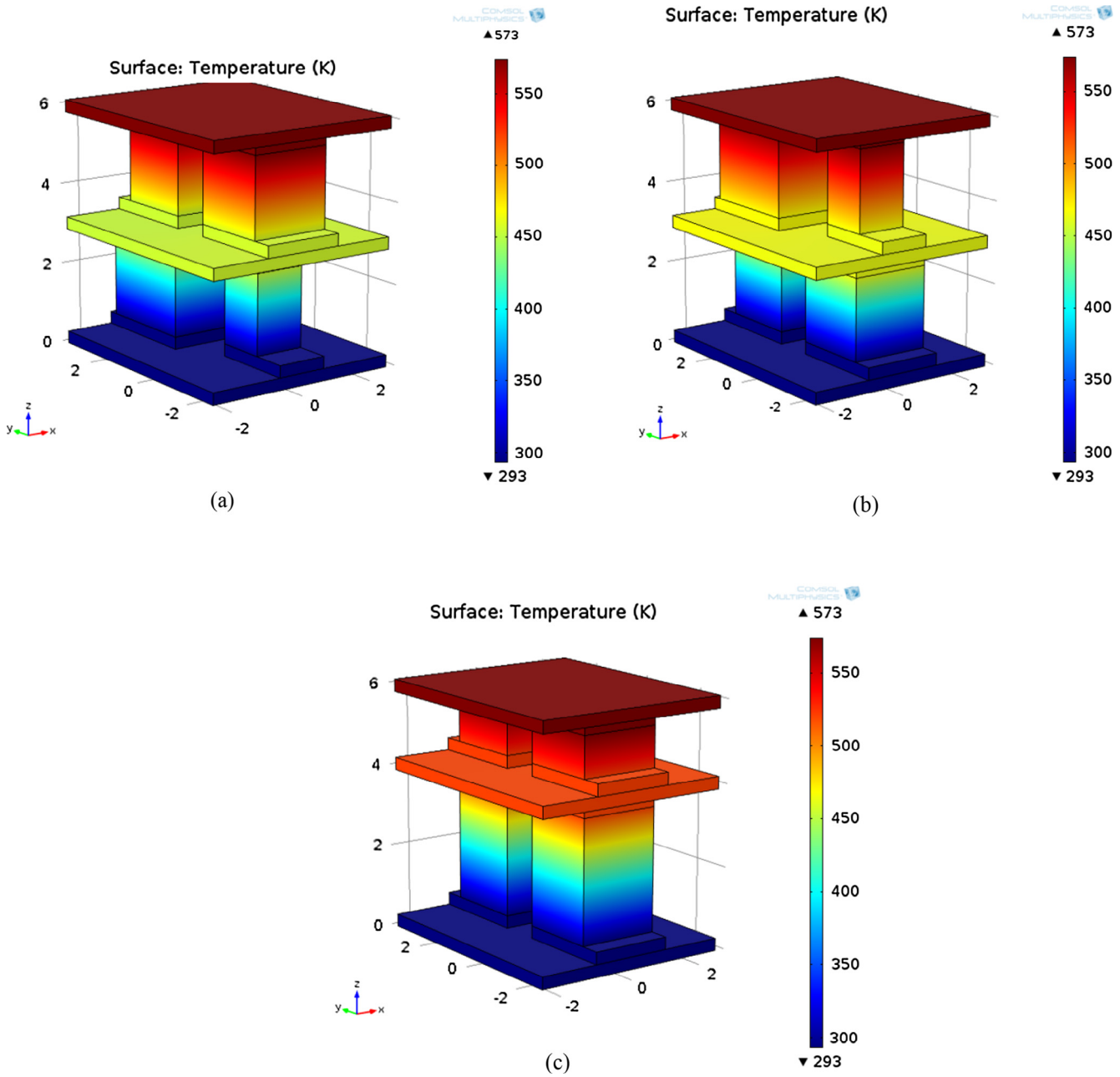

Fig. 2. 3D temperature distribution in uni-couple: (a) $\gamma_L = 0.25$, $\gamma_U = 1$, $H_{pnL} = 2$ mm, $H_{pnU} = 2$ mm; (b) $\gamma_L = 1$, $\gamma_U = 0.25$, $H_{pnL} = 2$ mm, $H_{pnU} = 2$ mm; (c) $\gamma_L = 1$, $\gamma_U = 1$, $H_{pnL} = 3$ mm, $H_{pnU} = 1$ mm.

3. Results and discussion

For the two-stage TEG uni-couple, the footprints of the n- and p-elements ($A_n + A_p$) were fixed at 8 mm^2 for each stage. The area of the identified ceramic substrate for each thermoelectric element was 5 mm × 6 mm. This module was selected as the test example to demonstrate the applicability of the proposed multi-objective and multi-parameter optimization approach for TEG geometry design. Because of the dependence of power output and conversion efficiency on the temperature, the optimal geometry of the TEG module should vary at different temperatures. Therefore, search variables with initial values of $H_{pn} = 2$ mm, $\gamma_L = 1$, and $\gamma_U = 1$ were optimized simultaneously to determine the optimal geometry at different temperatures from 200 to 700 °C. The selected hot-side temperatures represented low-, medium-, and high-temperature differences. In the following discussions, the single-objective optimization was presented before the multi-objective optimization to show the advantages of the latter method.

3.1. Single-objective optimization

3.1.1. Power as an optimization objective

To determine P_{opt} and η_{opt} in the multi-objective function (Eq. (1)), two single-objective optimizations were first implemented with power output and conversion efficiency as the objective functions, respectively. Figs. 4 and 5 show the evolutions of power output and conversion efficiency during optimization when power output was taken as the objective function. Power output significantly improved as the three search variables were optimized and finally reached a maximum value (Fig. 4), while conversion

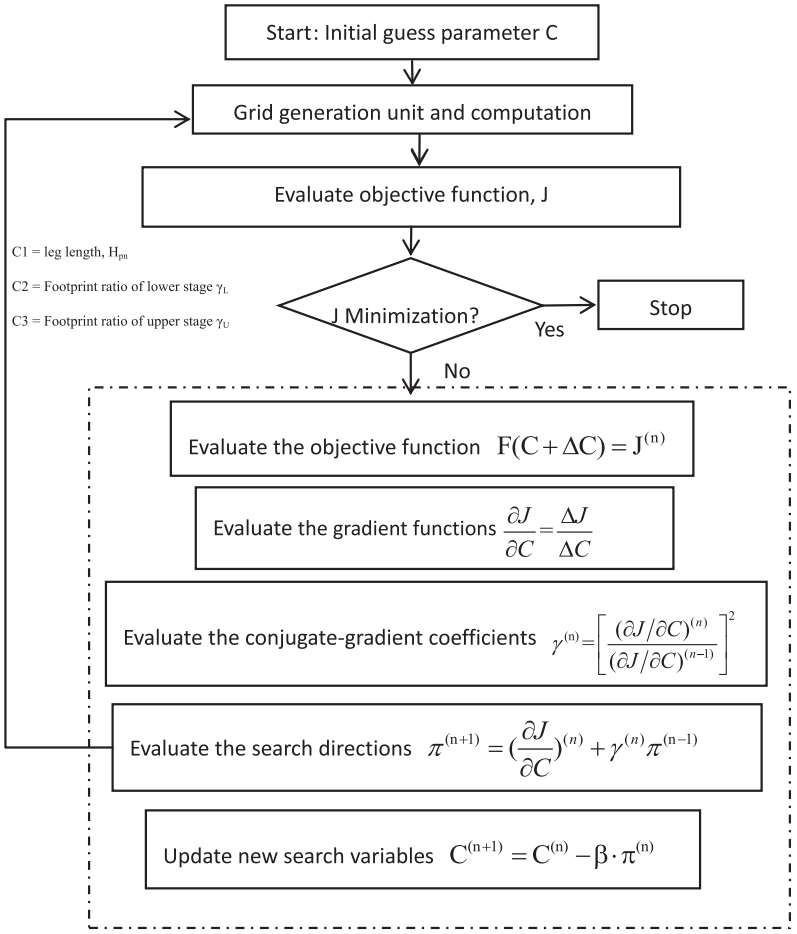

Fig. 3. Simplified conjugate-gradient method.

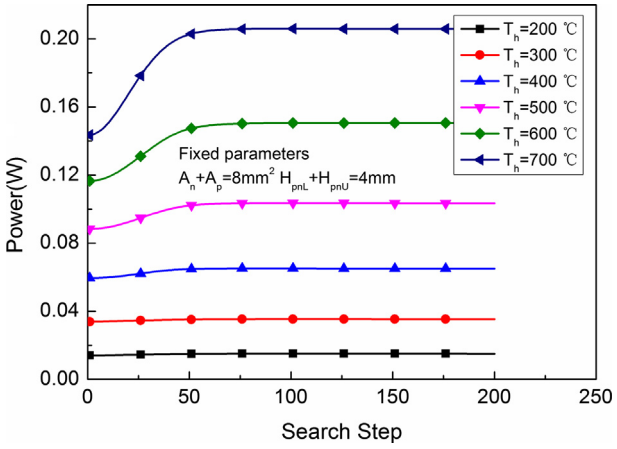

Fig. 4. Variations in TEG performance during optimization of P: power.

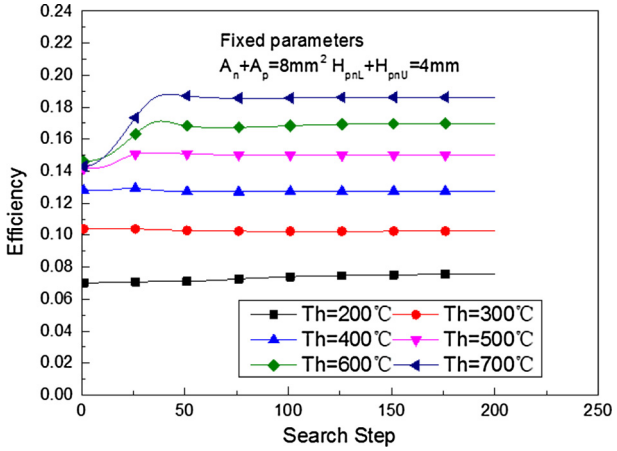

Fig. 5. Variations in TEG performance during optimization of P: η.

efficiency increased or decreased depending on the hot-side temperature (Fig. 5). When the TEG uni-couple reached the optimal design, power output significantly improved at 500, 600, and 700 °C by approximately 18.2%, 29.3%, and 43.3%, respectively, compared to the initial design. However, power output only increased by 7.1%, 5.3%, and 9.8% at 200, 300, and 400 °C, respectively. Fig. 5 shows that, when power output was taken as the objective function, the conversion efficiency of the optimal design showed two different trends depending on the hot-side temperature. At low and medium hot-side temperatures (200, 300, and 400 °C), the conversion efficiency of the optimal design was 7.55%, 10.25%, and 12.74%, respectively. These results are similar to the initial design values of 7%, 10.38%, and 12.8%, respectively. However, at high hot-side temperatures (500, 600, and 700 °C), the conversion efficiency of the optimal design was 15%, 16.9%, and 18.62%. These values were higher than the initial design values of 14.3%, 14.6%, and 14.29%, respectively. This means that it is possible to simultaneously increase the conversion efficiency and

power output. Hence, multi-objective optimization is necessary and feasible.

At low and medium temperatures below 500 °C, the power output and conversion efficiency of the optimal design were similar to the values of the initial design as expected. However, at high temperatures (500, 600, and 700 °C), the power output and conversion efficiency improved significantly and simultaneously. This occurred mainly for two reasons: first, when the thermoelectric materials and temperature difference were specified, the difference between the maximum conversion efficiency for the TEG modules with various designs was relatively small; second, the initial design of the TEG module reached or approached the maximum power output at these high temperatures, so the space for improvement in power output was small.

Figs. 6–8 show the evolutions of the three search variables during optimization. The optimal design depended on the hot-side temperature. The optimal designs are shown in Table 1.

Figs. 9–14 show the power and efficiency of each stage's evolutions during optimization when T_h = 200, 400, and 700 °C. For a low hot-side temperature, a material with a low working temperature, such as BiTe, is suitable. The increases in the total power and total efficiency were mainly the result of using BiTe as a fabrication material, as using skutterudite would result in losses in efficiency and power. However, at a high hot-side temperature, a material with a high working temperature such as skutterudite is better. Here, the increases in the total power and efficiency were mainly the result of the use of skutterudite as a fabrication material, as using BiTe would result in losses in efficiency and power. At medium hot-side temperatures, the use of BiTe or skutterudite as fabrication material had the same effect on power and efficiency.

3.1.2. Efficiency as an optimization objective

Figs. 15 and 16 show the evolutions in power output and conversion efficiency during optimization when conversion efficiency was the objective function. Significant improvements in conversion efficiency were observed as the three search variables were optimized and converged to a maximum value (Fig. 15). Meanwhile, power output increased or decreased depending on the hot-side temperature (Fig. 16). When the TEG uni-couple reached the optimal design at 200, 600, and 700 °C, the conversion efficiency significantly improved by 13.2%, 17.3%, and 31.6%, respectively, compared to the initial design. However, at 300, 400, and 500 °C, the conversion efficiency only increased by 1.06%, 1.1%, and 5.9%, respectively. This is because the initial TEG module designs reached or approached the maximum conversion efficiency at the hot-side temperatures, so the space for improvement in the conversion efficiency was small.

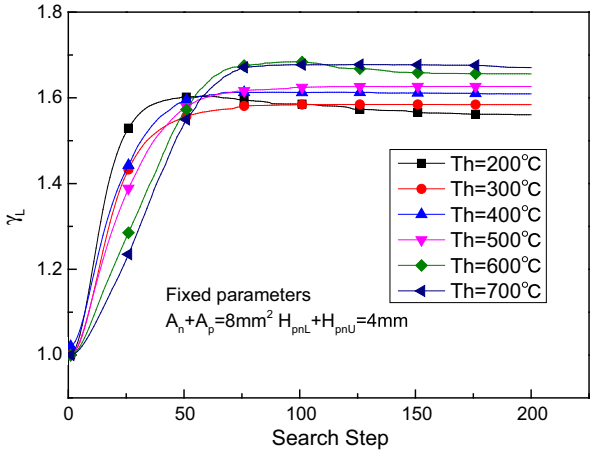

Fig. 6. Variations in TEG performance during optimization of P: γ_L.

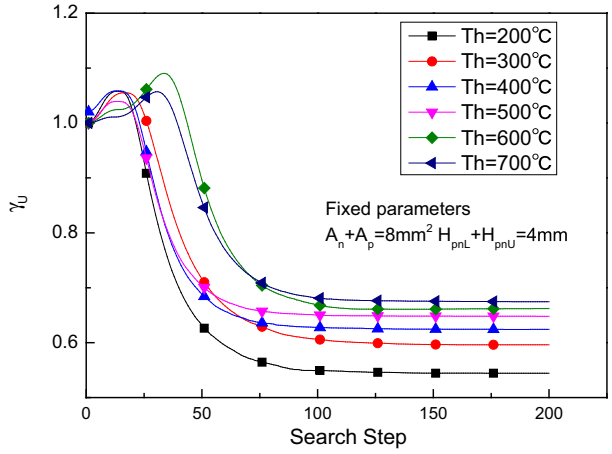

Fig. 7. Variations in TEG performance during optimization of P: γ_U.

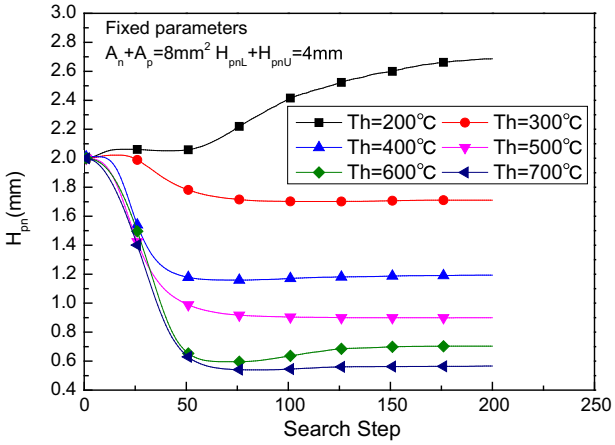

Fig. 8. Variations in TEG performance during optimization of P: H_{pn}.

Table 1
Optimal designs under different hot-side temperatures with power as an optimization objective.

T_h (°C)	H_{pn} (mm)	γ_L	γ_U
200	2.66	1.56	0.55
300	1.71	1.58	0.597
400	1.19	1.61	0.624
500	0.90	1.63	0.648
600	0.68	1.67	0.661
700	0.564	1.68	0.675

Fig. 16 shows that when conversion efficiency was the objective function, the power output of the optimal design presented two different trends depending on the hot-side temperature. At low and medium hot-side temperatures (200, 300, 400, and 500 °C), power output of the optimal design was 0.0149, 0.0342, 0.0605, and 0.0942 W, respectively. These values were only slightly higher than the initial design values of 0.014, 0.0338, 0.0594, and 0.0873 W, respectively. However, at high hot-side temperatures (600 and 700 °C), the power output of the optimal design was 0.1332 and 0.1774 W, respectively. These values were much higher than the initial design values of 0.1168 and 0.1440 W, respectively, with increases of 14% and 23.2%, respectively. Some power was sacrificed when the conversion efficiency was maximized at high

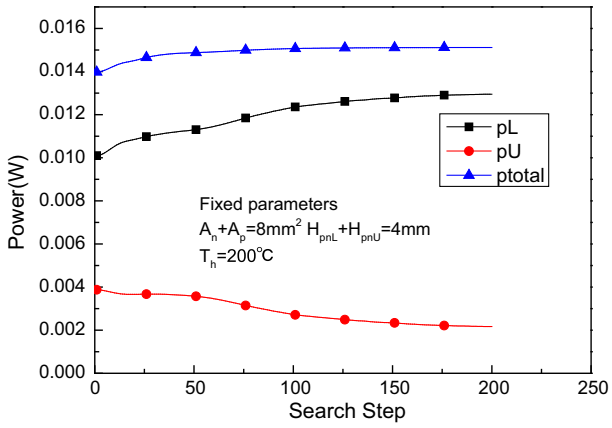

Fig. 9. Variations in TEG performance during optimization of P at T_h = 200 °C: P.

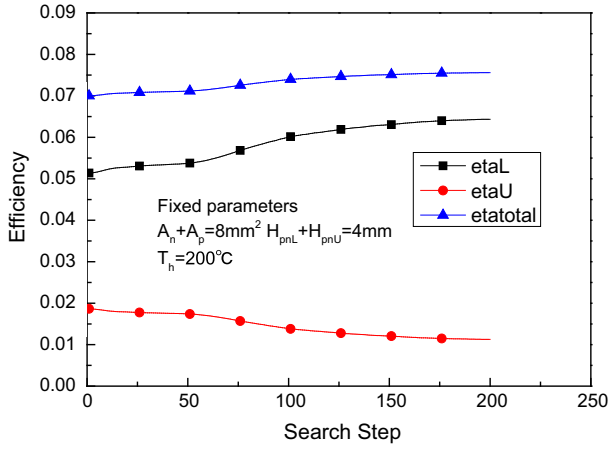

Fig. 10. Variations in TEG performance during optimization of P at T_h = 200 °C: η.

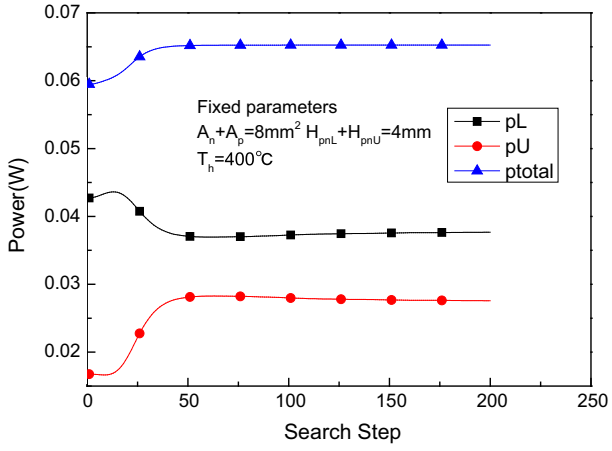

Fig. 11. Variations in TEG performance during optimization of P at T_h = 400 °C: P.

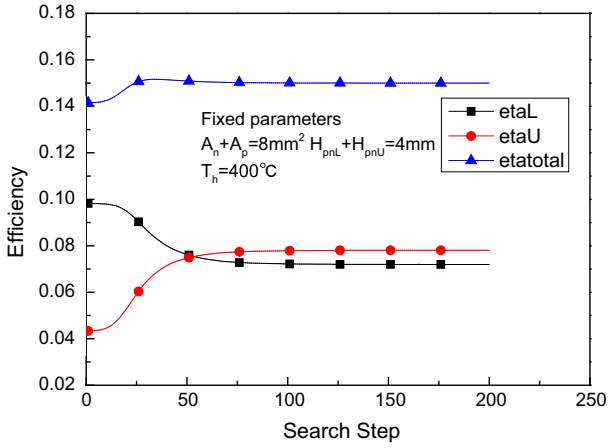

Fig. 12. Variations in TEG performance during optimization of P at T_h = 400 °C: η.

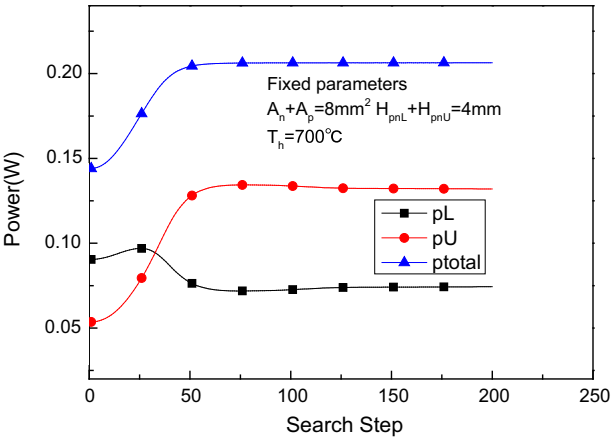

Fig. 13. Variations in TEG performance during optimization of P at T_h = 700 °C: P.

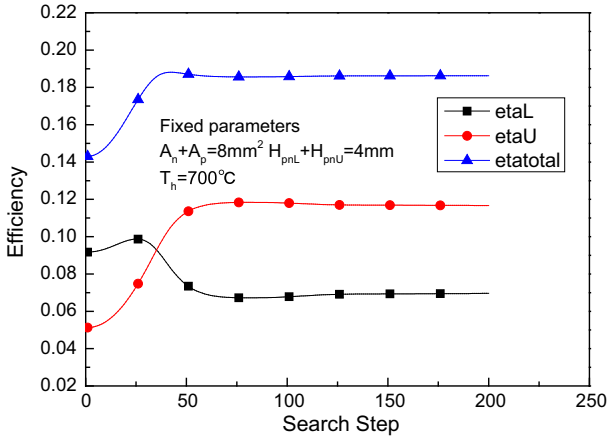

Fig. 14. Variations in TEG performance during optimization of P at T_h = 700 °C: η.

temperatures. These results again confirm that multi-objective optimization is necessary.

Figs. 17–19 show the evolutions of the three search variables during optimization at different temperatures. The optimal design depended on the hot-side temperature. The optimal designs are shown in Table 2.

Figs. 20 and 21 show the evolutions in power output and conversion efficiency of each stage during optimization when T_h = 400 °C. The results are similar to those of power output as an objective function.

3.2. Multi-objective optimization

Power output and conversion efficiency were taken as multi-objective functions. The single-objective optimization usually

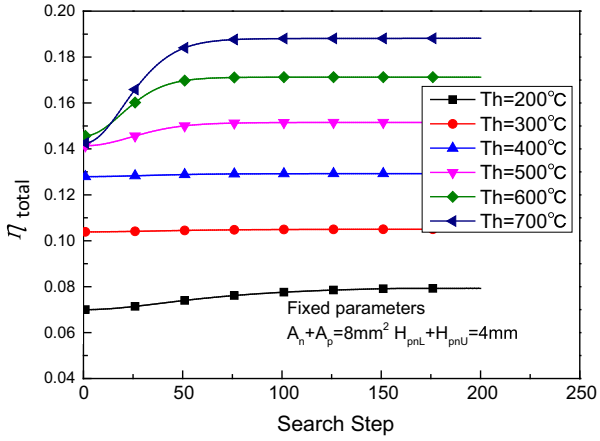

Fig. 15. Variations in TEG performance during optimization of η: η.

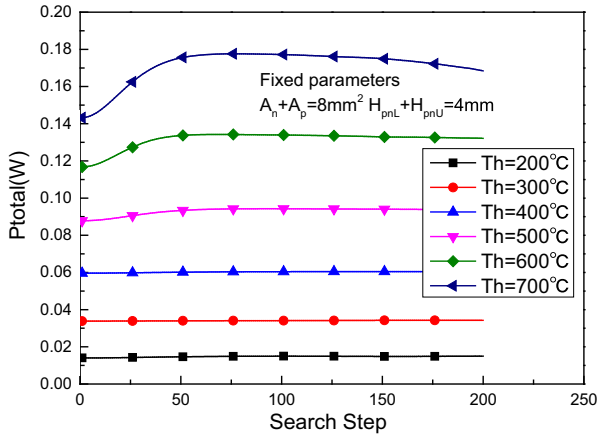

Fig. 16. Variations in TEG performance during optimization of η: P.

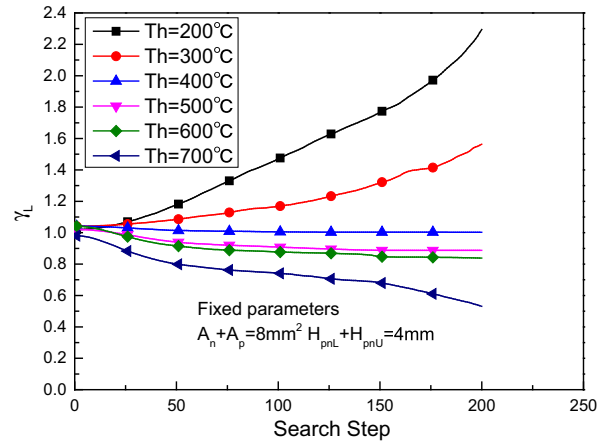

Fig. 17. Variations in TEG performance during optimization of η: γ_L.

improved power output at the cost of conversion efficiency and vice versa. Therefore, multi-objective optimization was implemented to enhance power output and conversion efficiency simultaneously. Note that the weight factor f in Eq. (1) may vary between 0 and 1, and any value gives relative importance to the single-objective function. The value of the weight factor can be selected by the designer; we adopted a value of 0.5.

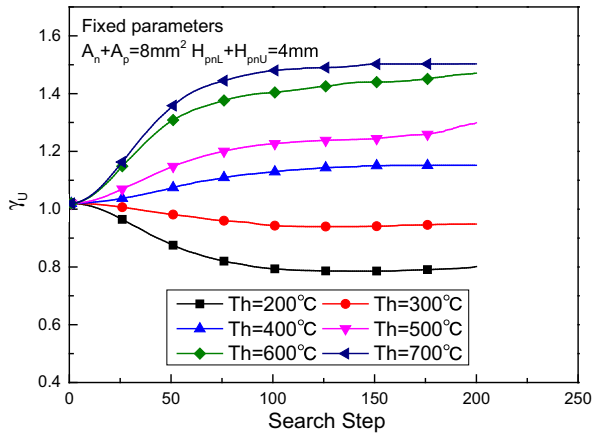

Fig. 18. Variations in TEG performance during optimization of η: γ_U.

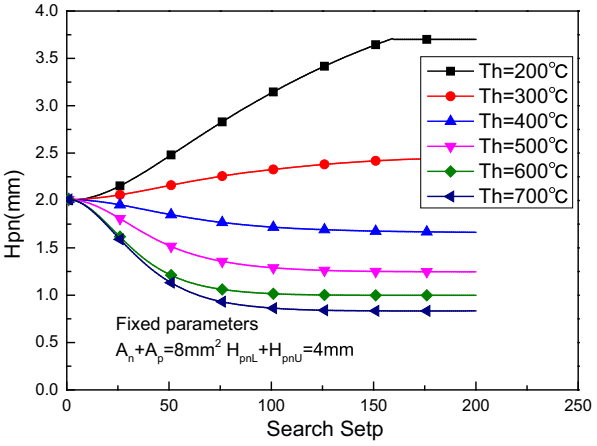

Fig. 19. Variations in TEG performance during optimization of η: H_{pn}.

Table 2
Optimal designs under different hot-side temperatures with efficiency as an optimization objective.

T_h (°C)	H_{pn} (mm)	γ_L	γ_U
200	3.7	2.06	0.793
300	2.42	1.329	0.941
400	1.67	1.003	1.152
500	1.283	0.905	1.223
600	0.999	0.864	1.437
700	0.876	0.748	1.474

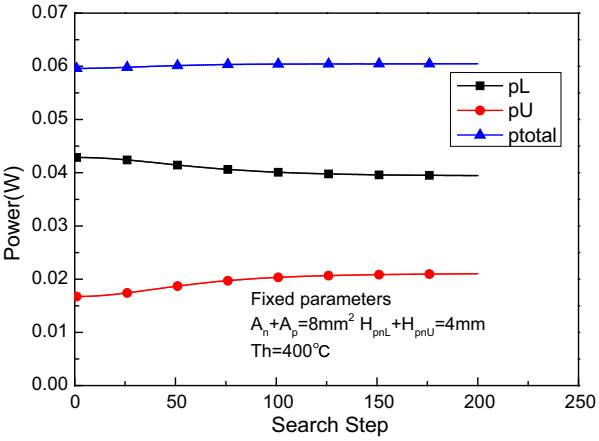

Fig. 20. Variations in TEG performance during optimization of η at T_h = 400 °C: P.

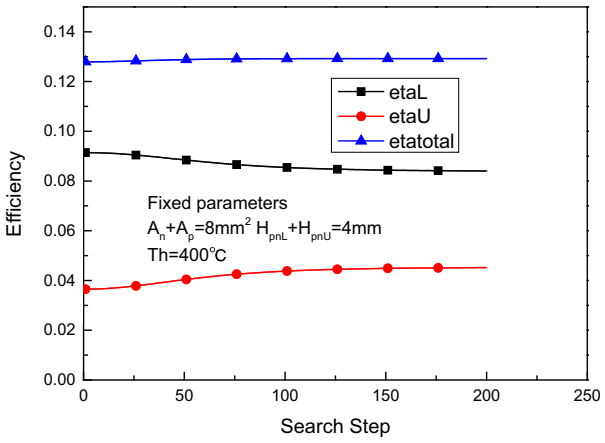

Fig. 21. Variations in TEG performance during optimization of η at T_h = 400 °C: η.

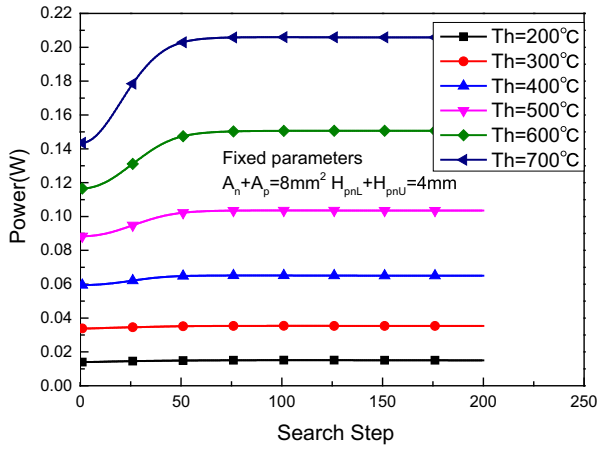

Fig. 22. Variations in TEG performance during multi-objective optimization: P.

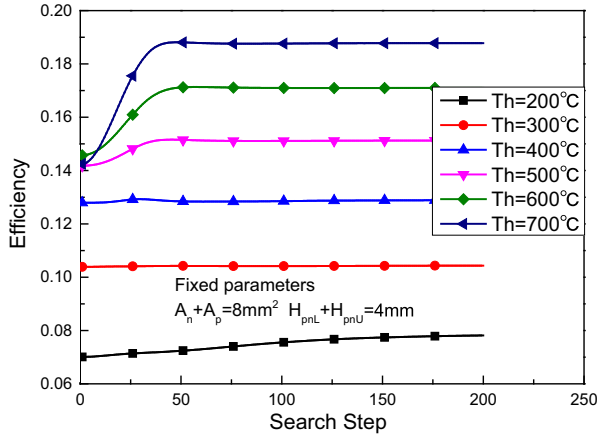

Fig. 23. Variations in TEG performance during multi-objective optimization: η.

Figs. 22 and 23 show the evolutions in power output and conversion efficiency of the TEG uni-couple during the multi-objective optimization.

At T_h = 500, 600, and 700 °C, power output significantly improved by 18.9%, 28.9%, and 30.6%, respectively, compared to the initial designs. However, at T_h = 200, 300, and 400 °C, the conversion efficiency only increased by 7.1%, 5.0%, and 9.4%, respectively. The optimal conversion efficiency at T_h = 200, 300, 400, 500, 600, and 700 °C was 7.8%, 10.43%, 12.89%, 15.13%, 17.1%, and 18.77%, respectively. The initial design conversion efficiency values were 7%, 10.39%, 12.80%, 14.3%, 14.6%, and 14.29%, respectively. At T_h = 200, 600, and 700 °C, the conversion efficiency significantly improved by 11.4%, 17.1%, and 31.4%, respectively, compared to the initial designs. However, at T_h = 300, 400, and 500 °C, the conversion efficiency only increased by 0.5%, 0.5%, and 5.6%, respectively, for two reasons. First, when the thermoelectric materials and temperature difference were specified, the differences between the maximum conversion efficiency and the power output of the TEG modules with various designs were relatively small. Second, the initial design of the TEG module reached or approached the maximum conversion efficiency and power output at these geometrics, hence, the space for improvement in conversion efficiency and power output was small.

Table 3 shows the optimal design with different objectives. A comparison of the results shows that the multi-objective optimization produced a reasonable balance between the power output and the conversion efficiency to improve both simultaneously.

Table 4 shows the detailed parameters of optimal design with different objectives. The optimal designs with multi-objective optimization required $1.5 < \gamma_L < 1.7$ and $0.5 < \gamma_U < 0.7$ for most of the hot-side temperatures, while the single-objective optimizations required much wider ranges of γ_L and γ_U for most of the hot-side temperatures than those for multi-objective optimization if η is the object.

Figs. 24–27 show the evolutions in the power outputs and efficiencies of the lower stage (P_L and η_L, respectively) and upper stage (P_U and η_U, respectively) of the TEG module during the multi-objective optimization. Because the length and area of the thermoelectric elements were fixed, the optimal design had to be a compromise between the lower and upper stages at different hot-side temperatures. For a lower hot-side temperature, the module must use more BiTe, and for a higher hot-side temperature, more skutterudite must be used. This is why the length of H_{pn} increased with the hot-side temperature.

Figs. 26 and 27 show the evolution in the efficiency. The efficiency of the lower stage was below a certain value. This was mainly because BiTe as a fabrication material does not work well above 300 °C.

Figs. 28 and 29 compare the T_h-P and T_h-η curves of the initial and optimal TEG uni-couple designs. The multi-objective optimization not only significantly elevated the power output but also improved the conversion efficiency. The maximum increases in power output and conversion efficiency occurred at T_h = 700 °C: 42.9% and 31.4%, respectively.

Table 3
Optimal design with different objectives.

	Initial design		η as objective		P as objective		Multi-objective	
T_h (°C)	P (W)	η	P (W)	η	P (W)	η	P (W)	η
200	0.0140	0.0700	0.0149	0.0793	0.0151	0.0755	0.0150	0.0780
300	0.0337	0.1038	0.0342	0.1050	0.0355	0.1025	0.0355	0.1043
400	0.0595	0.1280	0.0605	0.1293	0.0653	0.1274	0.0651	0.1289
500	0.0871	0.1430	0.0942	0.1515	0.1038	0.1500	0.1036	0.1513
600	0.1168	0.1460	0.1332	0.1713	0.0151	0.1690	0.1506	0.1710
700	0.1440	0.1429	0.1774	0.1880	0.2064	0.1862	0.2058	0.1877

Table 4
Parameters of optimal design with different objectives.

	P as objective			η as objective			Multi-objective		
T_h (°C)	H_{pn} (mm)	γ_L	γ_U	H_{pn} (mm)	γ_L	γ_U	H_{pn} (mm)	γ_L	γ_U
200	2.66	1.56	0.55	3.7	2.06	0.7793	3.23	1.54	0.52
300	1.71	1.58	0.597	2.42	1.329	0.941	2.02	1.56	0.58
400	1.19	1.61	0.624	1.67	1.003	1.152	1.38	1.59	0.61
500	0.90	1.63	0.648	1.283	0.905	1.223	1.03	1.62	0.64
600	0.68	1.67	0.661	0.999	0.864	1.437	0.81	1.64	0.66
700	0.564	1.68	0.675	0.8776	0.748	1.474	0.66	1.67	0.67

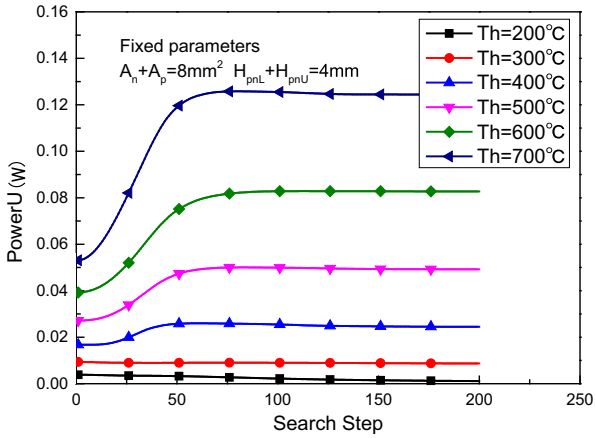

Fig. 24. Variations in TEG performance during multi-objective optimization: power of upper stage.

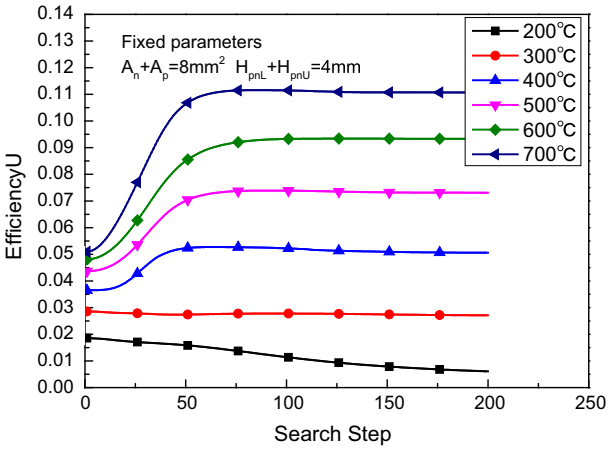

Fig. 26. Variations in TEG performance during multi-objective optimization: efficiency of upper stage.

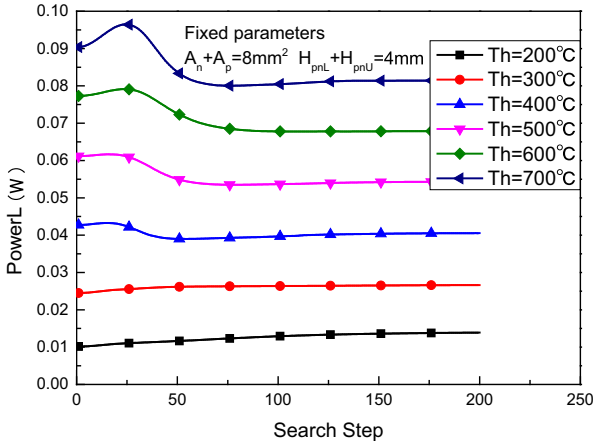

Fig. 25. Variations in TEG performance during multi-objective optimization: power of lower stage.

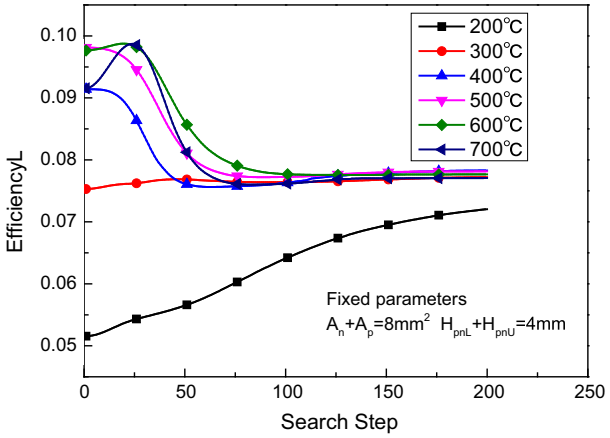

Fig. 27. Variations in TEG performance during multi-objective optimization: efficiency of lower stage.

The design of a TEG module can benefit from the references [6,41–44], however, further thorough experiments should be carried out to verify the results obtained by simulation before they can be used in industrial applications. In the future experimental work, the two-stage TEG modules as shown in Fig. 1 with different materials and geometrical parameters should be designed. Although it is not practical to test as many cases as we did in the optimizations, at least several representing cases are needed to verify the tendencies obtained by the optimizations.

4. Conclusions

This study presented an optimization approach for the design of a TEG module. In this approach, the direct problem solver adopted a multi-physics TEG model that was solved with COMSOL. The inverse problem solver used an SCG algorithm and was solved with MATLAB. The optimization approach was tested for both a BiTe- and a skutterudite-based two-stage TEG module. The element length was 2 mm with a cross-sectional area of 2×2 mm^2 for both the n- and p-type thermoelectric elements of each stage.

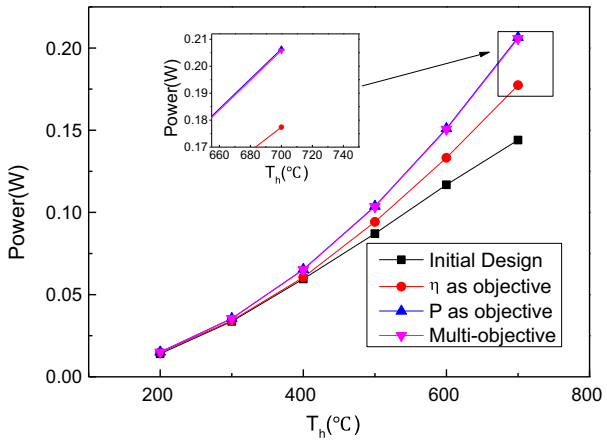

Fig. 28. Comparison of TEG power outputs of initial and optimal designs.

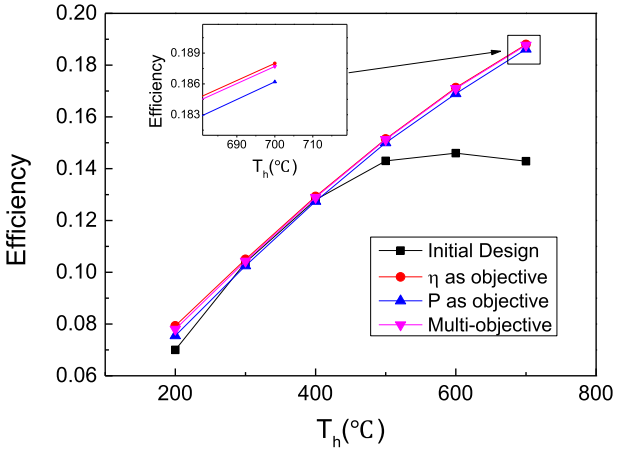

Fig. 29. Comparison of TEG efficiencies of initial and optimal designs.

Single-objective and multi-objective optimizations were implemented to determine the optimal TEG performance. Three geometric parameters were chosen as the search values and optimized simultaneously: the leg length of the lower stage H_{pn} and the footprint ratios of the lower and upper stages, γ_L and γ_U, respectively.

When the power output was the objective function, it was significantly elevated by the optimization of the three geometric parameters. The power outputs of the optimal design were about 5.7%, 5.0%, 9.4%, 18.9%, 28.9%, and 30.6% higher, respectively, than the initial design values. However, the improvement in power output reduced the conversion efficiency. Similarly, when the conversion efficiency was taken as the objective function, its increase in the optimal design was accompanied by a significant reduction in power output.

Thus, multi-objective optimization was necessary to improve power output and conversion efficiency simultaneously. The results confirmed the feasibility of the proposed multi-objective optimization approach. A weight factor of 0.5 produced a reasonable balance for improving power output and conversion efficiency simultaneously. The optimization results can be used to increase both the power output and efficiency of real thermoelectric systems such as solar thermoelectric systems.

Acknowledgements

This work was financially supported by the National Natural Science Foundation of China (No. 51376069) and the National Key Basic Research Program of China (973 Program) (No. 2013CB228302).

References

[1] Chen W-H, Wang C-C, Hung C-I, Yang C-C, Juang R-C. Modeling and simulation for the design of thermal-concentrated solar thermoelectric generator. Energy 2014;64:287–97.
[2] DiSalvo FJ. Thermoelectric cooling and power generation. Science 1999;285:703–6.
[3] Rowe D. Thermoelectric power generation. Electr Eng Proc Inst Electr Eng 1978;125:1113–36.
[4] He W, Wang S, Lu C, Zhang X, Li Y. Influence of different cooling methods on thermoelectric performance of an engine exhaust gas waste heat recovery system. Appl Energy 2016;162:1251–8.
[5] Kim H, Kim W. A way of achieving a low $/W and a decent power output from a thermoelectric device. Appl Energy 2015;139:205–11.
[6] Kwan TH, Wu X. Power and mass optimization of the hybrid solar panel and thermoelectric generators. Appl Energy 2016;165:297–307.
[7] Zhang T. New thinking on modeling of thermoelectric devices. Appl Energy 2016;168:65–74.
[8] Chiloyan V, Zeng L, Huberman S, Maznev AA, Nelson KA, Chen G. Variational approach to extracting the phonon mean free path distribution from the spectral Boltzmann transport equation. Phys Rev B 2016;93:155201.
[9] Chiloyan V, Zeng L, Huberman S, Maznev AA, Nelson KA, Chen G. Variational approach to solving the spectral boltzmann transport equation in transient thermal grating for thin films. arXiv preprint arXiv:160508007; 2016.
[10] Hu Y, Zeng L, Minnich AJ, Dresselhaus MS, Chen G. Spectral mapping of thermal conductivity through nanoscale ballistic transport. Nat Nanotechnol 2015;10:701–6.
[11] Zeng L, Chen G. Disparate quasiballistic heat conduction regimes from periodic heat sources on a substrate. J Appl Phys 2014;116:064307.
[12] Zeng L, Chiloyan V, Huberman S, Maznev AA, Peraud J-PM, Hadjiconstantinou NG, et al. Monte Carlo study of non-diffusive relaxation of a transient thermal grating in thin membranes. Appl Phys Lett 2016;108:063107.
[13] Zeng L, Collins KC, Hu Y, Luckyanova MN, Maznev AA, Huberman S, et al. Measuring phonon mean free path distributions by probing quasiballistic phonon transport in grating nanostructures. Sci Rep 2015:5.
[14] Riffat SB, Ma X. Thermoelectrics: a review of present and potential applications. Appl Therm Eng 2003;23:913–35.
[15] Wang Y, Chiao S, Lai MT, Yang SY. The role of polycarbonate molecular weight in the poly (L-lactide) blends compatibilized with poly (butylene succinate-co-L-lactate). Polym Eng Sci 2013;53:1171–80.
[16] Weng C-C, Huang M-J. A simulation study of automotive waste heat recovery using a thermoelectric power generator. Int J Therm Sci 2013;71:302–9.
[17] Liang X, Sun X, Tian H, Shu G, Wang Y, Wang X. Comparison and parameter optimization of a two-stage thermoelectric generator using high temperature exhaust of internal combustion engine. Appl Energy 2014;130:190–9.
[18] O'Brien R, Ambrosi R, Bannister N, Howe S, Atkinson HV. Safe radioisotope thermoelectric generators and heat sources for space applications. J Nucl Mater 2008;377:506–21.
[19] Chen G. Theoretical efficiency of solar thermoelectric energy generators. J Appl Phys 2011;109:104908.
[20] Chen J, Lin B, Wang H, Lin G. Optimal design of a multi-couple thermoelectric generator. Semicond Sci Technol 2000;15:184.
[21] Chen L, Li J, Sun F, Wu C. Performance optimization of a two-stage semiconductor thermoelectric-generator. Appl Energy 2005;82:300–12.
[22] Meng F, Chen L, Sun F. Multivariable optimization of two-stage thermoelectric refrigerator driven by two-stage thermoelectric generator with external heat transfer. Indian J Pure Appl Phys 2010;48:731–42.
[23] Meng F, Chen L, Sun F. A numerical model and comparative investigation of a thermoelectric generator with multi-irreversibilities. Energy 2011;36:3513–22.
[24] Wang C-C, Hung C-I, Chen W-H. Design of heat sink for improving the performance of thermoelectric generator using two-stage optimization. Energy 2012;39:236–45.
[25] Jang B, Han S, Kim J-Y. Optimal design for micro-thermoelectric generators using finite element analysis. Microelectron Eng 2011;88:775–8.
[26] Huang Y-X, Wang X-D, Cheng C-H, Lin DT-W. Geometry optimization of thermoelectric coolers using simplified conjugate-gradient method. Energy 2013;59:689–97.
[27] Meng J-H, Zhang X-X, Wang X-D. Multi-objective and multi-parameter optimization of a thermoelectric generator module. Energy 2014;71:367–76.
[28] Rezania A, Yazawa K, Rosendahl L, Shakouri A. Co-optimized design of microchannel heat exchangers and thermoelectric generators. Int J Therm Sci 2013;72:73–81.
[29] Yazawa K, Shakouri A. Cost-efficiency trade-off and the design of thermoelectric power generators. Environ Sci Technol 2011;45:7548–53.
[30] Minnich A, Dresselhaus M, Ren Z, Chen G. Bulk nanostructured thermoelectric materials: current research and future prospects. Energy Environ Sci 2009;2:466–79.
[31] Jang J-Y, Tsai Y-C. Optimization of thermoelectric generator module spacing and spreader thickness used in a waste heat recovery system. Appl Therm Eng 2013;51:677–89.

[32] Rowe D, Min G. Evaluation of thermoelectric modules for power generation. J Power Sources 1998;73:193–8.
[33] Wang X-D, Huang Y-X, Cheng C-H, Lin DT-W, Kang C-H. A three-dimensional numerical modeling of thermoelectric device with consideration of coupling of temperature field and electric potential field. Energy 2012;47:488–97.
[34] Tan G, Wang S, Tang X. Thermoelectric performance optimization in p-type CeyFe3CoSb12 skutterudites. J Electron Mater 2014;43:1712–7.
[35] Yang J, Hao Q, Wang H, Lan Y, He Q, Minnich A, et al. Solubility study of Yb in n-type skutterudites Ybx Co 4 Sb12 and their enhanced thermoelectric properties. Phys Rev B 2009;80:115329.
[36] Decher R. Direct energy conversion: fundamentals of electric power production. Oxford University Press; 1997.
[37] Bitschi A. Modelling of thermoelectric devices for electric power generation: Diss., Eidgenössische Technische Hochschule ETH Zürich, Nr. 18441, 2009; 2009.
[38] Lesage FJ, Pagé-Potvin N. Experimental analysis of peak power output of a thermoelectric liquid-to-liquid generator under an increasing electrical load resistance. Energy Convers Manage 2013;66:98–105.
[39] Kim HS, Kikuchi K, Itoh T, Iida T, Taya M. Design of segmented thermoelectric generator based on cost-effective and light-weight thermoelectric alloys. Mater Sci Eng, B 2014;185:45–52.
[40] Lesage FJ, Pelletier R, Fournier L, Sempels ÉV. Optimal electrical load for peak power of a thermoelectric module with a solar electric application. Energy Convers Manage 2013;74:51–9.
[41] Gou X, Xiao H, Yang S. Modeling, experimental study and optimization on low-temperature waste heat thermoelectric generator system. Appl Energy 2010;87:3131–6.
[42] Hyland M, Hunter H, Liu J, Veety E, Vashaee D. Wearable thermoelectric generators for human body heat harvesting. Appl Energy 2016;182:518–24.
[43] Arora R, Kaushik SC, Arora R. Multi-objective and multi-parameter optimization of two-stage thermoelectric generator in electrically series and parallel configurations through NSGA-II. Energy 2015;91:242–54.
[44] Chen J, Zuo L, Wu Y, Klein J. Modeling, experiments and optimization of an on-pipe thermoelectric generator. Energy Convers Manage 2016;122:298–309.